

# 1 An Explainable Machine Learning Based Flashover Prediction Model Using Dimension- 2 Wise Class Activation Map

3 Linhao Fan<sup>a</sup>, Wai Cheong Tam<sup>b\*</sup>, Qi Tong<sup>c</sup>, Eugene Yujun Fu<sup>d</sup>, Tianshui Liang<sup>a\*</sup>

4 <sup>a</sup>School of Mechanics and Safety Engineering, Zhengzhou University, Zhengzhou, China,  
5 tree7fan@gs.zzu.edu.cn, liangtsh@zzu.edu.cn \*

6 <sup>b</sup>Fire Research Division, National Institute of Standards and Technology, 100 Bureau Drive,  
7 Gaithersburg, Maryland, USA, waicheong.tam@nist.gov

8 <sup>c</sup>Department of Civil and Systems Engineering, Johns Hopkins University, Baltimore,  
9 Maryland, USA, qtong5@jhu.edu

10 <sup>d</sup>The Hong Kong Polytechnic University, Hung Hom, Hong Kong, eugene.fu@polyu.edu.hk

11 \*Corresponding author

## 12 13 **Highlights:**

- 14 • A deep-learning (DL) model was developed to simultaneously predict flashover with  
15 lead time.
- 16 • Synthetic temperature data for more than 17 000 fire cases were used to develop the  
17 DL model.
- 18 • Dimension-wise Class Activation Map is utilized to interpret models for increasing  
19 trustworthiness of the DL model.
- 20 • The proposed model was tested on 11 full-scale experimental data to assess its  
21 prediction capability in real fire scenarios.

## 22 23 **Abstract:**

24 This paper presents the development of an explainable machine learning based flashover  
25 prediction model, named xFlashNet. Synthetic temperature data from more than 17 000 fire  
26 cases are used for model development. The effect of missing data due to heat detectors to  
27 elevated temperature from the fire scene is also considered. xFlashNet utilizes multi-residual  
28 convolutional layers to effectively learn the indicative temperature features and dimension-  
29 wise class activation map (dCAM) to interpret the model decision. The proposed model is  
30 benchmarked against three current-state-of-the-art models. Results shows that the proposed  
31 model outperforms the benchmark models and it has an overall accuracy of about 92.9 %.  
32 Based on dCAM, the model decision is analyzed. Depending on the location of the fire and the  
33 heat detector operating conditions, the proposed model shows the discriminative region of the  
34 temperature inputs which influence the model to make the decision. In addition, model testing  
35 against real fire data is conducted. It is believed that this present work contributes a step  
36 forward to bring trustworthy ML systems to fire safety applications and to enhance situational  
37 awareness for firefighting safety that can help reduce firefighter injuries and deaths.

38  
39 **Keywords:** flashover occurrence; machine learning; explainable multivariate series  
40 classification; real-time prediction; smart firefighting

## 1 **1. Introduction**

2 Current home structure fires are more hazardous. In a recent study [1], it is experimentally  
3 shown that flashover occurs in a much shorter time from a fire in a modern room consisting of  
4 synthetic materials. By definition [2], flashover is an extreme fire phenomenon in which a local  
5 fire rapidly transitions into full room involvement. Physically, almost all combustible materials  
6 in an enclosed space are ignited simultaneously. In this situation, the resulting average  
7 temperature of the enclosed space can exceed 800 °C from approximately 100 °C in less than  
8 30 seconds [3]. At this point, personal protective equipment is highly unlikely to provide  
9 effective protections to the firefighters and they must retreat before the flashover occurs. Based  
10 on previous studies [2, 3], it is well established that if the average temperature of the hot gas  
11 layer reaches approximately 550 °C to 650 °C and/or the average incident heat flux onto the  
12 floor surface is about 20 kW/m<sup>2</sup> to 25 kW/m<sup>2</sup>, flashover is likely to occur. However, this kind  
13 of information is difficult to be obtained on a fire scene. In fact, firefighters can only rely on  
14 their experience to recognize flashover indicators, such as rollover [4], to avoid flashover.  
15 Since the fire growth the fire scene is complex and highly dynamic and with the fact that the  
16 onset of flashover to yield a full room involvement takes less than 30 seconds, if the firefighters  
17 are unable to recognize the potential occurrence of flashover in advance, their lives will be in  
18 great danger.

19 In the past twenty years, attempts were made to develop models that can be used to predict the  
20 onset of flashover. For example, Babrauskas [3] presented an empirical formula to predict the  
21 occurrence of flashover using a simple combustion model. Mccaffrey et al. [5] developed a  
22 simple method for estimating the likelihood of the occurrence of flashover in an enclosure.  
23 Kim and Lilley [6] found that the major influential factors for flashover in a space are the fire  
24 growth rate and the ventilation opening area. However, these empirical formulas were limited  
25 to simple geometric configurations with a single compartment and a door-like opening. In order  
26 to accommodate multi-compartment structures, Jahn [7] used computational fluid dynamic  
27 (CFD) based fire simulation model to predict the future temperatures. The transient heat release  
28 rate of the fire was estimated using real-time temperature readings from sensors. But there were  
29 two major problems. The first problem is that the exact fire location and the interior door  
30 opening conditions are needed. However, in real fire scenarios, this kind of information is  
31 generally unknown. The second problem is that the CFD based approach requires extremely  
32 long computational time and the use of high performance computers. It was noted from [7] that  
33 a single calculation takes more than five minutes to complete. For that, it can be seen that the  
34 traditional prediction methods are not numerically efficient at providing real-time decision-  
35 making assistance to firefighters in complex fire scenarios.

36 Recent studies show that the machine learning (ML) paradigm can be a promising tool to  
37 overcome the numerical challenges from real-life practical engineering applications. This  
38 robust technology has been used in fault detection [8], human activity recognition [9], structural  
39 health monitoring [10] and other engineering field [11,12]. These ML-based models are  
40 formulated with close-form mathematical expressions and since these models are always  
41 trained/developed beforehand, they are easy to use and are extremely numerically efficient. In

1 the fire research community, the ML paradigm has also been utilized in various prediction  
2 tasks. Wang et al. [13] proposed a support vector regression to recover missing temperature in  
3 the room of fire origin using temperature information from other rooms. Wu et al. [14] used a  
4 long-short term memory to estimate the location and size of the original fire source in a tunnel.  
5 Kou et al. [15] developed a model based on gated recurrent unit to determine the fire location  
6 and its growing intensity in complex building structure. Fu et al. [16] utilized an attention based  
7 bi-directional long short-term memory to predict future occurrence of flashover in a single-  
8 story family home. Zhang et al. [17] proposed a stacked long short-term memory to predict the  
9 onset of flashover in a 0.5 m by 0.5 m compartment. Results from these studies [13-17]  
10 demonstrated that if the ML-based model is designed properly, it can effectively learn the  
11 indicative patterns from the data and is capable of providing reliable predictions in less than a  
12 second without the need of prior knowledge about the fire location and other boundary  
13 conditions.

14 Despite the numerical advantages from [13-17], there is one sufficient drawback of using the  
15 ML paradigm and that is, the models are not explainable. Often times, it is considered as a  
16 black box. It is well understood that being able to explain the model decision is important for  
17 practical engineering applications, especially when the potential applications involve lives.  
18 Also, model interpretability provides traceable information to scientists or engineers to  
19 understand the underlying reasons why a model is making such a correct or a wrong decision.  
20 In this study, an explainable ML-based flashover prediction model is proposed and the model  
21 interpretability is introduced using a technique called dimension-wise Class Activation Map  
22 (dCAM) [18]. Unlike the traditional CAM [19] in which it can only extract spatially average  
23 information in the temporal domain, dCAM offers discriminative information in both spatial  
24 and temporal domains for the multivariate series. Specifically, when a decision is made by the  
25 ML-based model, the model also outputs a weight for each element of the input sequence. It is  
26 believed that this research work contributes a crucial step to enhance explainable ML and to  
27 bring trust for utilizing ML-based technologies in fire safety problems.

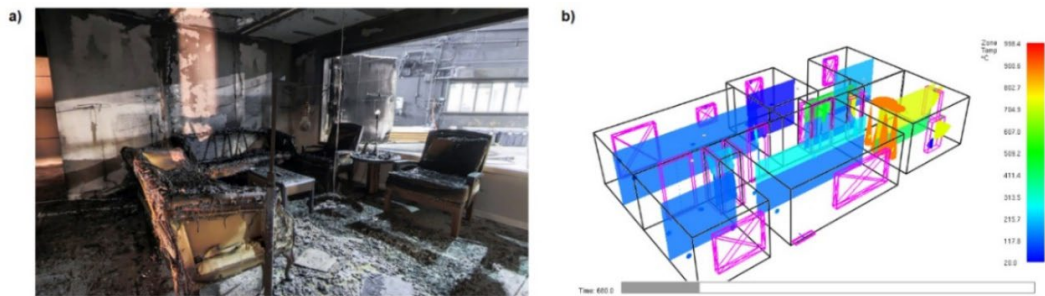
28 The rest of the paper is organized as follows. Section 2 describes the data collection process  
29 for temperature data involving flashover using a learning-by-synthesis approach, numerical  
30 setup of the problem, data behaviors, data preprocessing, and potential challenges. Section 3  
31 presents the development of the explainable deep learning based flashover prediction model  
32 and the formulation of the dimension-wise class activation map. Then, Section 4 provides the  
33 model assessment against current state-of-the-art models, parametric studies on the effect of  
34 missing temperature to the model performance, and model interpretability for visualizing the  
35 discriminant regions with dCAM. Finally, Section 5 presents the conclusions of this study.

## 36 **2. Flashover Temperature Data Collection Process**

37 Training a ML model using a deep learning algorithm requires a large amount of relevant data.  
38 This requirement is due to the fact that deep learning algorithms need data to extract useful  
39 features to carry out the prediction task. However, obtaining temperature data from real-life  
40 full-scale fire tests in a residential home [20] involving flashover as shown in Fig. 1a is  
41 challenging, costly, and time-consuming. It was shown in [13] that approximately 3000 fire

1 cases are needed to develop a converged model for a simple three-compartment building  
2 structure. For that, in order to obtain a sufficient amount of temperature data for the  
3 development of a ML based flashover prediction model, the learning-by-synthesis approach  
4 [21] was used in this study. Basically, this approach relies on utilizing a fire simulation  
5 computer program to conduct numerical experiments with various fires such that a synthetic  
6 temperature dataset can be obtained for model development.

7 CFAST Data generator (CData) [22] was used to obtain the desired amount of temperature data  
8 from various fire and venting opening conditions in a residential home. The description of the  
9 residential home is provided in the subsequent section and an example of a simulation run is  
10 shown in Fig. 1b. CData uses CFAST as the simulation engine. CFAST is a two-zone fire  
11 model that predicts the thermal environment caused by a fire within a compartmented structure.  
12 In general, CFAST has been validated against more than 15 other sets of full-scale experiments  
13 [23] with peak heat release rate (HRR), compartment aspect ratio (i.e., compartment length  
14 against ceiling height), and global equivalence ratio, ranging from approximately 50 kW to  
15 15 700 kW, 0.4 to 4.9, and roughly 0 to a value larger than 1 for a wide range of ventilation  
16 factors, respectively. For the residential home considered in this study, a separate validation  
17 case study (gas burner) based on the settings from [20] was conducted and the absolute error  
18 between the predicted upper layer gas temperature from CFAST and the experiment  
19 measurements was about 6 %. From that, CFAST is reliable to generate synthetic temperature  
20 data to facilitate the current study.



21  
22 Fig. 1. a) Screenshot of the full-scale experiment from the residential home [20] and b)  
23 CFAST simulation run for the residential home.

## 24 2.1 Numerical Setup

25 Figure 2a shows a single-story residential home. As seen in the figure, there are seven different  
26 compartments: a kitchen (K), a dining room (DR), a living room (LR), three bedrooms (B1,  
27 B2, B3), and a hallway (HW). The overall approximate interior dimensions of the structure are  
28 13.92 m (x-direction)  $\times$  7.7 m (y-direction) with a ceiling height of 2.44 m. The detailed  
29 dimensions associated with each of the compartments are shown in Fig. 2a. The walls and  
30 ceiling of each compartment are constructed using gypsum wallboard and the floor material is

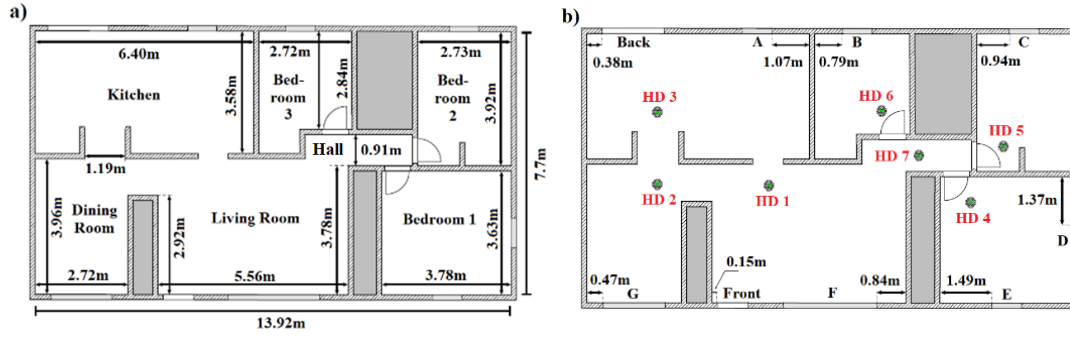


Fig. 2. Overview of a) the single story structure and b) openings with heat detectors (HD).

Fig. 2b shows the relative position of the openings and the heat detectors in different compartments. For the openings, there are two exterior doors (front and back), three bedroom doors, and seven windows (A through G). All windows are constructed using 3-mm single-layer float glass. The vent sizes and sill heights are summarized in Table 1. There is one heat detector in each compartment and they are located approximately 0.02 m down from the ceiling. The heat detectors are used to collect the temperature near the ceiling in each compartment.

Table 1. Summary of approximate vent size and sill height (unit in m) [20].

Vents	Front	Back	A	B	C	D	E	F	G
Tall	2.05	2.05	1.02	1.46	1.46	1.46	1.46	1.46	1.46
Width	0.89	1.78	0.85	0.86	0.86	0.86	0.85	2.67	1.78
Sill Height	0	0	1.07	0.61	0.61	0.61	0.61	0.61	0.61

## 2.2 Fire Conditions

Three fire effects, namely fire growth, fire location, and nearby-item ignition, are taken into account to specify the fire conditions. Firstly, the fire growth of the first ignited item is described by a four-stage HRR curve. Fig. 3a shows that the fire undergoes a linear fire growth, t-squared fire growth, peak, and a decay stage. Three furnishing items, such as a sofa, cotton-based mattress, and a polyurethane based mattress, are considered. Table 2 shows the corresponding values for the smoldering to flaming fire ( $Q_L$ ), peak HRR ( $Q_{max}$ ), time to transition ( $t_L$ ), time to peak HRR ( $tp1$ ), peak time ( $tp2 - tp1$ ), and decay time ( $t_E - tp2$ ) and these values are determined based on the reported experimental work from [24, 25]. In general, this fire configuration provides different fires with the growth rate ranging between slow, medium, and fast.

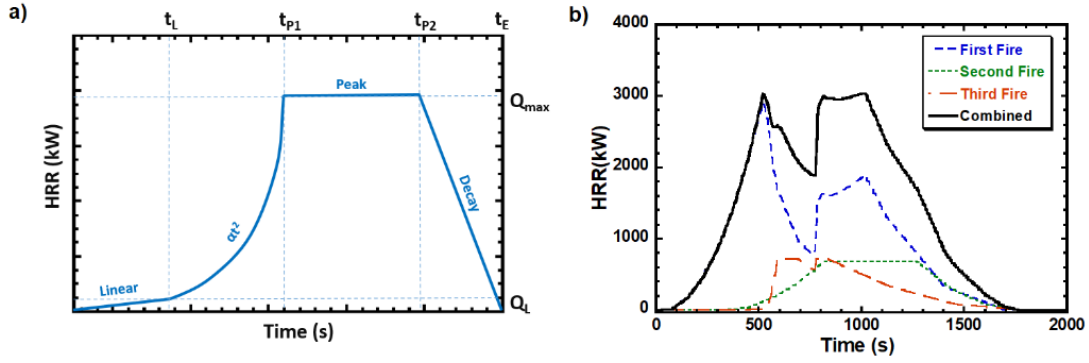


Fig. 3. a) Four-stage fire growth curve and b) an example of a fire case.

Table 2. HRR parameters for burning items.

$Q_L$ (kW)	$Q_{max}$ (kW)	$t_L$ (s)	$t_{P1}$ (s)	$t_{P2}-t_{P1}$ (s)	$t_E-t_{P2}$ (s)
10 – 30	270 – 3500	50 – 150	50 – 300	0 – 500	100 – 1070

Secondly, there is one fire in each fire case. The fire is assumed to be initiated on the floor surface in either LR, K, or B1 and the fire is located in the middle of these compartments about 0.5 m away from the left wall. Thirdly, in order to account for more complex fire growth behaviors, ignition up to two additional fires is considered. In CFAST, two targets are placed about  $\pm 0.725$  m (in y-direction) away from the first fire with its normal facing the first fire. The ignition criterion is determined based on the incident heat flux onto the targets and the value of the ignition heat flux ranges from 20 kW/m<sup>2</sup> to 50 kW/m<sup>2</sup>. Once the ignition criterion is met, a secondary fire occurs. This fire is also described by the four-stage fire curve and Fig. 3b shows an example of multi-item ignition. It is expected that this fire setting can offer simulation cases with various fire growth behaviors. It should be noted that the noticeable change of HRR curve from the first fire is discussed in below section.

### 2.3 Vent Opening Conditions

Two types of vent-opening conditions are considered. The first type is the time-trigger vent opening condition, which is applied to the front door and three bedroom doors. For the current study, each of these doors is initially closed. At the beginning of the numerical experiment, each door has 50 % chance to be opened. The intents of this type of vent opening condition are to mimic simple door opening events due to evacuation and to obtain temperature data that captures various effects due to air exchange between different compartments and oxygen availability.

The second type is the temperature-trigger setting and it allows windows to be arbitrarily opened when a temperature threshold is reached. This is because due to temperature or a flux gradient [26], a window may crack and eventually break out creating an opening to the outside environment. Based on [27], breakage of a single-pane float glass is experimentally observed at temperature between 100 °C and 200 °C. In CFAST, a target is placed at the top of a window to create the window breakage phenomenon. When the temperature of a target reaches a threshold, the corresponding window will then be opened. As shown in Fig. 3b, the HRR drops

1 at about 500 s due to lack of oxygen in the fire compartment. The window from that  
 2 compartment breaks at about 800 s. It can be seen that when fresh air enters the compartment,  
 3 the HRR from the first fire increases. It is believed that the vent opening settings help to account  
 4 for simulation cases with different fire growth behaviors. Table 3 provides the summary of the  
 5 parameters for data generation in this study. Uniform sampling function is used to generate the  
 6 fire cases.

7 Table 3. The summary of parameters considered in the data generation process.

Parameters	Fire Conditions			Vent Opening Conditions	
	Fire location	HRR	Nearby-item ignition criterion	Probability of door opening	Triggering temperature for window opening
Range of Values	Living Room, Kitchen, Bedroom 1	See Table 2	20 kW/m <sup>2</sup> - 50 kW/m <sup>2</sup>	50%	100 °C – 200 °C

8

9 **2.4 Data Behavior and Data Preprocessing**

10 Sixty-thousand numerical experiments with a wide range of fire and vent opening conditions  
 11 are conducted. Of these experiments, there are only 17 365 fire cases that have reached the  
 12 flashover condition. Based on the literature from [2,3], it is assumed that the flashover  
 13 condition is met when the upper layer gas temperature of the compartment reaches 600 °C.  
 14 This flashover condition also being used in various flashover prediction studies [3,5,13]. The  
 15 duration of each numerical experiment is 3600 s with an output temperature interval of 5 s.  
 16 Temperature profiles for each heat detector (HD) and the upper layer gas temperature from the  
 17 room of fire origin are recorded. It should be noted that in order to ensure the data balance in  
 18 between non-flashover and flashover data, only the fire cases with the occurrence of flashover  
 19 are being used. This is because flashover fire cases have both the non-flashover and flashover  
 20 data whereas the non-flashover fire cases only have the non-flashover data.

21 Fig. 4a shows the HD temperature of each compartment from a medium fire growth case that  
 22 is shown in Fig. 3b. The second and third items are ignited at around 300 s, and 400 s,  
 23 respectively and have relatively different fire growth rates. The upper layer temperature from  
 24 B1 is denoted as an indicator because this temperature profiles is only used for labeling the  
 25 data and is not used for model training. The visualization of the simulation case can also be  
 26 seen in Fig. 1b. The front door and the B3 door are always closed. As seen from the temperature  
 27 profiles in Fig. 4a, the heat from B1 spreads across the hallway, then to LR and B2, and to the  
 28 dining room and kitchen. This set of temperature profiles is used to described how the data  
 29 instances for each flashover fire case are formulated.

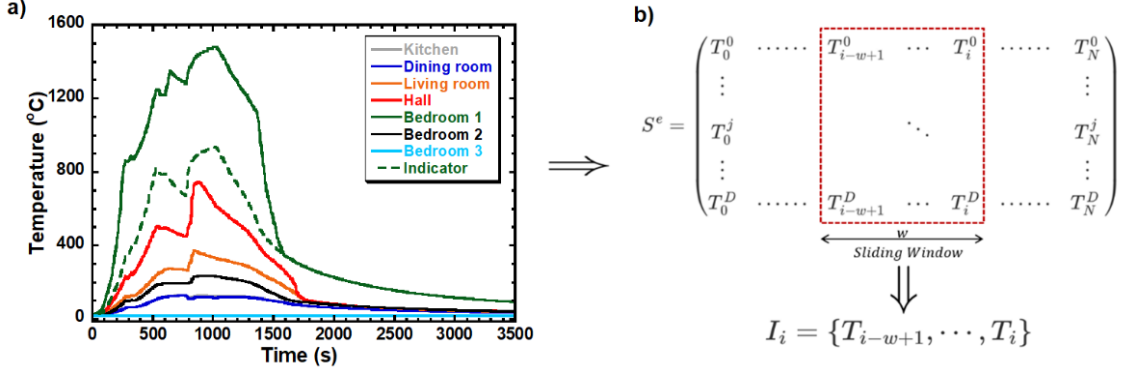


Fig. 4. a) Temperature profiles for a flashover fire case and b) an illustration of a sliding window with a window size of  $w$ .

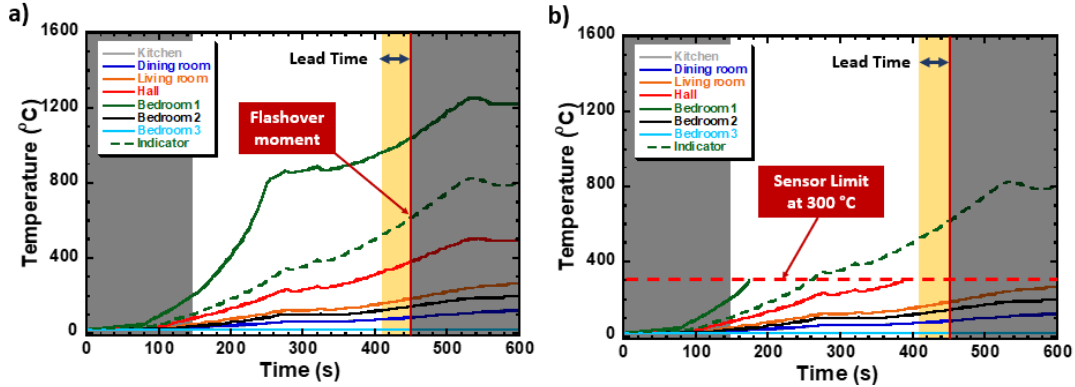
In order to carry out model training, instances need to be extracted from each flashover fire case. Two parameters, namely sliding window and lead time, are considered for instance extraction. The sliding window is used to facilitate real-time continuous predictions. Fig. 4b shows an illustration of a data sequence with a sliding window of size  $w$ . For that, a single input instance,  $I^e$ , consists of temperature data from each HD and it is denoted as  $I^e = [T_{i-w}^j, \dots, T_i^j]$  for  $j = 1, \dots, D$  where  $D$  is the total number of HD. Because firefighters need additional time to react, a lead time of 30 s is considered. With that, the model uses input instances up to present time to determine if there is a potential occurrence of flashover in 30 s. Given that, the input instance is rewritten as  $I^e = [T_{i-w-lt}^j, \dots, T_{i-lt}^j]$  where  $lt$  is the lead time.

In this study, the model performs a binary classification task and this means that the model predicts if there is no flashover or if there is a flashover in 30 s. For that, two separate sets of instances are needed to be obtained. Given the lead time of 30 s and the output temperature interval of 5 s, the current setting yields six flashover instances. Since the flashover moment (FO) is known for each flashover fire case, the flashover instance for 5 seconds before flashover is  $I_{FO-5}^e = [T_{FO-5-w}^j, \dots, T_{FO-5}^j]$  and the six flashover instances are  $I_{FO-i}^e$  where  $i = 30, 25, \dots, 10, 5$ . Since it is important to maintain data balance in between flashover and non-flashover data, six non-flashover data are obtained for each flashover case and they are  $I_{FO-i}^e$  where  $i = 60, 55, \dots, 40, 35$ . Therefore, the entire dataset has 208 380 instances (17 365 x 12).

## 2.5 Potential Challenges

In real-life fire scenarios, HDs cannot survive at elevated temperature and will be destroyed well below the flashover temperature conditions. Based on NFPA 72 [28], heat sensing fire detectors are categorized into seven different classes with temperature classifications ranging from low to ultra-high, and the maximum operational temperature ranges from approximately 29 °C to 302 °C. Fig. 5a shows the zoomed-in temperature profiles as shown in Fig. 4a and Fig. 5b shows the identical figure with a temperature cut-off at 300 °C. As seen in Fig. 5b, the lower the maximum operational temperature of the HDs, less temperature signals are available. With less temperature information, the prediction of the potential flashover occurrence will become more difficult. It can be seen that in addition to being able to discriminate temperature data with high importance, the model also needs to have learning capabilities to correlate

1 complex temperature information from other compartments to flashover conditions in the room  
 2 of fire origin. Therefore, a parametric study is conducted to understand the effect of maximum  
 3 operational temperature to the model performance.



4  
 5 Fig. 5. a) Zoom-in plot of Fig. 4a and b) temperature profiles of the same case with HD  
 6 maximum operational temperature at 300 °C.

### 7 3. Development of Explainable Flashover Neural Network Model (xFlashNet)

#### 8 3.1 Model structure

9 Fig. 6 shows the overall model structure of xFlashNet (explainable Flashover Neural network  
 10 model). The model consists of two main components. One component is a neural network to  
 11 correlate temperature data for predicting flashover events. The other component involves  
 12 utilizing the Class Activate Mapping (CAM) method to provide model interpretability for the  
 13 predictions and CAM is a post-processing method in which it does not participate in the training  
 14 process.

15 The model takes an input of multivariate time series,  $I_i \in \mathbb{R}^{D \times N}$ , where  $i$  is from 1 to  $M$  for  $M$ ,  
 16  $D$ , and  $N$  being the number of flashover cases, the number of heat detectors, and the length of  
 17 the temperature instance, respectively. The model has three residual blocks. Fig. 6b shows the  
 18 layer structure of the residual block and as seen, it contains three one-dimensional convolution  
 19 (1D Conv) layers and a residual connection. The use of 1D Conv is to extract features from  
 20 input instances [19]. The residual connection is included to stabilize model training and to  
 21 allow deeper networks from vanishing gradient [29]. Mathematically, the output features,  $h$ ,  
 22 from the first and the second convolutional layer,  $ConvB$ , is:

$$23 \quad h_i = Relu(ConvB_i(h_{i-1})) \quad \text{for} \quad i = 1 \text{ and } 2 \quad (1)$$

24 with

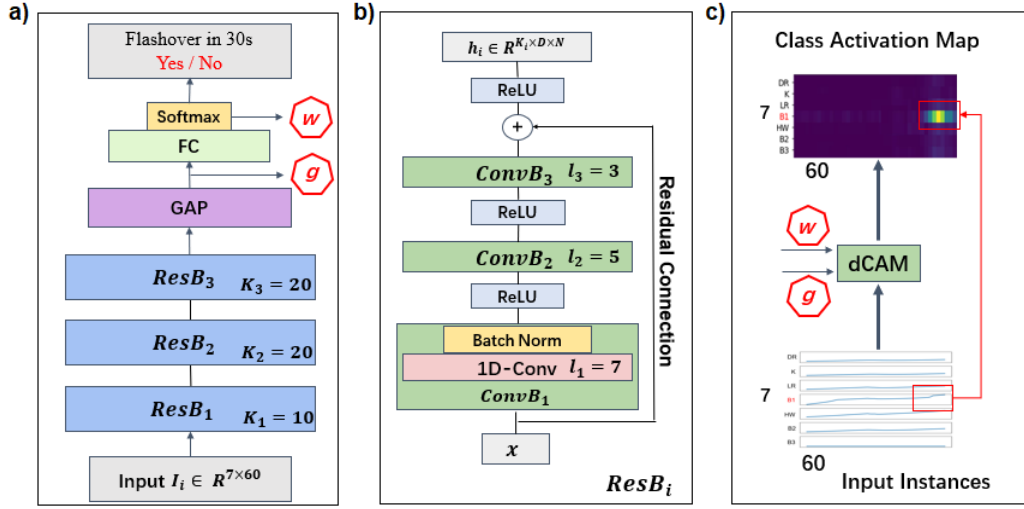
$$25 \quad ConvB_i(h_i) = BN(W_i \otimes h_i + b_i) \quad (2)$$

26 where  $h_0$  is the input information ( $x$ ),  $b$  is the bias vector,  $W$  is the weight matrix,  $\otimes$  is the  
 27 convolution operator/kernel, and  $BN$  is the batch normalization.  $BN$  is used to normalize the  
 28 extracted features from the convolution in the same scale. And ReLU (rectified linear unit  
 29 activation function) is utilized to include nonlinearity for feature activations (i.e., to determine

1 the importance of the features). The last convolutional layer extracts higher level features and  
 2 it is concatenated with the original input information from the beginning of the residual block:

$$3 \quad h_3 = \text{Relu}(\text{Conv}B_3(h_2) + h_0) \quad (3)$$

4 The kernel size ( $l_i$ ) and stride are determined based on numerical experiments and they are [7,  
 5 5, 3] and [1, 1, 1], for the first, second, and third convolution layers, respectively. The extracted  
 6 features from the first residual block are passed onto the subsequent residual blocks. The  
 7 convolution setting for each block is identical except the number of kernels. The convolution  
 8 from the first residual block has the kernel number of 10 and the convolution from the second  
 9 and third residual blocks have the kernel number of 20. The increase of kernel number in later  
 10 convolution layers is to allow the model to remember a larger number of higher level features  
 11 which are generally more useful for predictions.



12  
 13 Fig. 6. a) Overall model structure of xFlashNet, b) structure of a residual block, and c)  
 14 information flow to obtain the dimension-wise class activation map.

15 As shown from Fig. 6a, the feature representation is then passed to a global average pooling  
 16 (GAP) layer. Basically, GAP takes the average of the output feature representation from the  
 17 last residual block,  $h^3$ , in the temporal domain and it is obtained based on the following  
 18 expression:

$$19 \quad g(k) = \frac{1}{N * D} \sum_j^N \sum_i^D h^3(i, j, k) \quad \text{for } k = 1, 2, \dots, K^3 \quad (4)$$

20 where  $g$  is GAP output feature representation. It should be noted that the empty dimension  
 21 indicates the number of flashover fire cases in the training subset and the data assignment is  
 22 discussed in next subsection. Finally, the fully connected layer takes the feature representation  
 23 and a prediction,  $p$ , is given by:

$$24 \quad p = \text{softmax}(\sum_k^{K^3} (w_k * g_k + b_k)) \quad (5)$$

25 where  $w_k$  and  $b_k$  are the weight and bias of the fully connected layer, respectively. Softmax  
 26 activation function is used because this is a binary classification task such that the outputs are

1 probabilities ranging from 0 to 1. The final output for each fire case has an output dimension  
 2 of  $1 \times 2$  (i.e.,  $y = [0.17, 0.83]$ ). A prediction threshold of 0.5 is used to determine if the final  
 3 output is considered as non-flashover or flashover. Given  $y = [0.17, 0.83]$ , the prediction is  
 4 considered as flashover.

### 5 **3.2 Formulation of Dimension-Wise Class Activation Map (dCAM)**

6 Fig. 6c shows the illustration on how a dimension-wise class activation map (dCAM) is  
 7 obtained. In principle, a dCAM can be obtained for each input instance and it is shown in the  
 8 figure that the dCAM can be used to understand the most discriminative parts of the  
 9 multivariate temperature information (see the solid red boxes) that the model tends to focus to  
 10 make a prediction. It should be noted that the determination of the dCAM is a post-processing  
 11 process and the dCAM is obtained using the feature representations from the last residual block  
 12 and the weights from the fully connected layer from the final xFlashNet. The primary process  
 13 for obtaining the dCAM is presented below and readers who are interested in the derivation  
 14 and detailed explanation of dCAM can refer to [18].

15 Five steps are involved in order to obtain dCAM for each instance. Firstly, for a given data  
 16 instance  $I_i^j$  with  $i$  being the index of the temperature sequence (from 1 to 60) and  $j$  being the  
 17 index of the HD (from 1 to 7), a new input structure  $C(I)$  is formed:

$$18 \quad C(I) = \begin{bmatrix} I^D & I^1 & \dots & I^{D-2} & I^{D-1} \\ \vdots & \vdots & \dots & \vdots & \vdots \\ I^2 & I^3 & \dots & I^D & I^1 \\ I^1 & I^2 & \dots & I^{D-1} & I^D \end{bmatrix} \quad (6)$$

19  $C(I)$  has a dimension of  $D \times D \times N$  and as seen in Eqn.6, the first element of each row is offset  
 20 by one HD. The inclusion of an extra dimension in  $C(I)$ , rather than only using  $I_i^j$ , is to enable  
 21 the determination of the data importance in spatial domain and offsetting the elements of each  
 22 row allows subsequent random permutation calculations (an important step to find out the data  
 23 importance in temporal domain) without having duplicate inputs. The discussion on the random  
 24 permutation calculation is provided in the third step.

25 Secondly, a regular class activation map (CAM) is obtained for each sequential element of  
 26  $C(I)$  and the CAM is obtained as:

$$27 \quad CAM(I_i^j) = \sum_k^{K^3} w_k^c * g_k(I_i^j) \quad (7)$$

28 where  $g_k$  is feature representations from Eqn.4 and  $w_k^c$  is the weight matrix from Eqn.5 that  
 29 specifically belongs to the prediction class,  $c$ , which is non-flashover or flashover. It should be  
 30 noted that the activated weights for the two different classes are different. From Eqn.7, one can  
 31 see that different sequential orders of  $I_i^j$  in  $C(I)$  yield different  $CAM(C(I))$  and the  
 32 corresponding CAM might not be the most influential for model decision making in temporal  
 33 domain. For that, the random permutation calculation is carried out such that the temporal data  
 34 importance can be numerically determined.

35 Thirdly, a single permutation is denoted as  $S_I^1$ . For example, if  $I = \{I^1, I^2, I^3\}$ , one possible

1 permutation is  $S_I^1 = \{I^2, I^3, I^1\}$ . It can be seen that the possible permutation of  $C(I)$  for all  $I$   
 2 scales as  $D!$ . In the current study, since there are 7 HDs in the building structures, leading to 7  
 3 x 7 x 60 for  $C(I)$ , the possible permutation is  $7!$  which is 5040. This kind of brute force  
 4 approach does work, but it requires lengthy computational time. Based on [18], for  $D = 10$ , it  
 5 was numerically observed that the number of required permutations,  $z$ , is 100 to achieve  
 6 discriminative feature accuracy of about 90 %. From that, the number of permutations  
 7 considered in this study is taken to be 100 for  $S_I^z$  where  $z$  is from 1 to 100 and CAM is obtained  
 8 for all  $S_I^z$ . This yield 100 different CAM with the dimension of 7 x 7 x 60.

9 Fourthly, a mean CAM,  $\overline{CAM}(X_1, X_2, X_3)$ , over 100 possible CAMs is obtained, where  $X_1$ ,  
 10  $X_2$ , and  $X_3$  represent different sensors, the position of sensors, and the time dimension. This  
 11 averaging of CAMs provides a summarization of the importance of each element from  $C(I)$ .  
 12 Fig. 7 (most left) shows an example of  $\overline{CAM}$  and the red box in the most left part of the figure  
 13 shows the most discriminant subsequence. In general, this kind of interpretation is  
 14 counterintuitive because one would consider the high values (see the dotted box) are regarded  
 15 as discriminative. However, based on numerical observation, this type of high values has  
 16 relatively constant activation. With that, any changes to the data information for the  
 17 subsequence are not important and so the activations with strong variance indicate that any  
 18 missing information has much larger effects. Therefore, if the activation is low for a  $X_2$  in  
 19  $\overline{CAM}$  and high for  $X_2$ , then the subsequence at  $X_2$  has strong variance and is thus  
 20 discriminant.

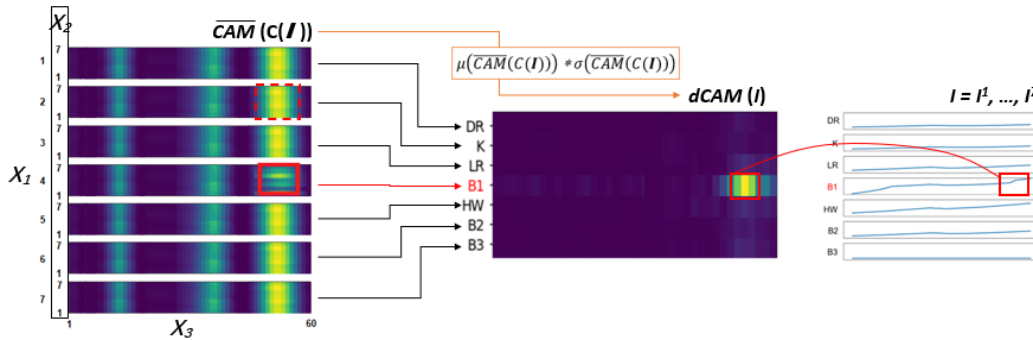


Fig. 7. dCAM determination process.

23 Lastly, given the CAM behaviors, dCAM is determined from the following expression:

$$24 \quad dCAM = \mu(\overline{CAM}(C(I))) * \sigma^2(\overline{CAM}(C(I))) \quad (8)$$

25 with  $\mu$  and  $\sigma$  are the mean and the standard derivation of  $\overline{CAM}(X_1, X_2, X_3)$  in  $X_2$   
 26 dimension. The final dCAM is in the dimension of  $D \times N$  and in this study, it is 7 x 60. The  
 27 middle of Fig.7 shows the dCAM for a particular flashover instance and by observing the  
 28 important region in dCAM, one can relate the corresponding input temperature (see right most  
 29 figure) that the model tends to focus on during decision marking. It should be noted that dark  
 30 blue and light yellow colors represent 0 and 1, respectively. In Section 4.3, three sets of  
 31 examples are provided to highlight the dCAM to achieve better model interpretability.

#### 32 4. Results and Discussion

## 1 4.1 Model Performance of xFlashNet

2 To demonstrate the performance of the model, three baseline models are selected for  
 3 benchmarking. These models include a feedforward multiple-layer perceptron (MLP) [30], a  
 4 two-layer long short-term memory (LSTM) [17], and a three-layer fully convolutional neural  
 5 network (FCN) [19]. Each model is fine-tuned to obtain optimal model performance. In order  
 6 to assess the model performance, three evaluation metrics, accuracy, precision and recall, are  
 7 used and they are determined from the following expressions:

$$8 \text{ Accuracy} = \frac{TP+TN}{TP+TN+FP+FN} \quad (10)$$

$$9 \text{ Precision} = \frac{TP}{TP+FP} \quad (11)$$

$$10 \text{ Recall} = \frac{TP}{TP+FN} \quad (12)$$

11 where TP, TN, FP, and FN are true positive, true negative, false positive, and false negative,  
 12 respectively. The testing subset (20 838 instances) is used in the following model evaluation.  
 13 The testing subset (20 838 instances) is used in the following model evaluation. All models are  
 14 tested on the same testing set to ensure consistency for model comparison.

15 Table 4 shows the performance of each model using inputs with a sliding window size of 300 s.  
 16 It can be seen that xFlashNet has the best prediction performance; it has a loss value of about  
 17 0.171 and an overall accuracy of about 92.9 %. In addition, xFlashNet has a relatively high  
 18 recall score and this is important because the model has fewer false negatives. Furthermore, it  
 19 is worth noting that xFlashNet has a lighter model structure with only 12 602 trainable  
 20 parameters. As compared to numerical performance reported in [7], xFlashNet needs less than  
 21 0.01 seconds to make a prediction and it can be seen that xFlashNet can meet the real-time  
 22 prediction requirements for practical firefighting applications.

23 Table 4. Model performance for xFlashNet and state-of-the-art models.

Model	Loss	Accuracy	Precision	Recall	Testing Time (s)	Trainable Parameters
MLP	0.467	84.1 %	80.4 %	90.3 %	1.42	16 658
LSTM	0.285	87.3 %	83.4 %	92.9 %	1.73	14 302
FCN	0.227	90.6 %	88.8 %	93.0 %	1.36	13 282
xFlashNet	0.171	92.9 %	91.6 %	94.4 %	1.69	12 602

24

## 25 4.2 Effect of Missing Data to xFlashNet Performance

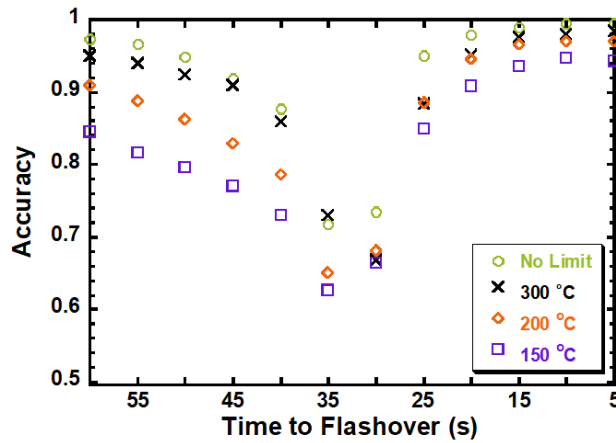
26 To investigate the model performance under realistic scenarios where the HD fails to provide  
 27 temperature data, a parameter study is conducted. Based on the descriptions provided in Section  
 28 2.5, three HD maximum operating temperature limits are considered: 300 °C, 200 °C, and  
 29 150°C. In a fire case, if the HD readings exceed the temperature limit, a non-realistic  
 30 temperature (i.e., 0 °C) is replaced. Table 5 shows the model performance of xFlashNet under  
 31 different HD failure limits. It can be seen from the table that the amount of available data

1 decreases with lower HD maximum operating temperature limits. Because there is less  
 2 temperature information, the model performance drops from about 92.9 % (ideal HD that never  
 3 fails) to approximately 81.9 % when HD fails at 150 °C.

4 Table 5. xFlashNet model performance from different HD temperature limits.

HD Temperature Limits	Loss	Acc.	Precision	Recall	Missing Temperature (%)
No limit	0.171	92.9 %	91.6 %	94.4 %	0 %
300 °C	0.246	89.6 %	88.7 %	90.7 %	16.8 %
200 °C	0.308	86.1 %	83.4 %	90.2 %	20.8 %
150 °C	0.384	81.9 %	78.7 %	87.4 %	29.2 %

5  
 6 To further understand the model performance, Fig. 8 presents the overall accuracy of each  
 7 instance for fire cases with different HD maximum operating temperature limits. It can be seen  
 8 that the overall accuracy tends to decrease for predictions of  $I_{FO-35}$  and  $I_{FO-30}$ . Practically,  
 9 this kind of model behavior is expected because the temperature data for these two instances  
 10 have similar temperature information, but they have completely different labels (the earlier  
 11 instance as non-flashover and the latter as flashover). With that, it is difficult for the model to  
 12 distinguish them. Yet, for  $I_{FO-20}$ , ...,  $I_{FO-5}$ , which are closer to the flashover moment, the  
 13 model accuracy improves. From the ideal HD cases (no limit), the accuracy is about 98 %. The  
 14 model performance is still promising (with an accuracy of about 90 %) even when the  
 15 temperature limit of the heat detector is set at 150 °C. Furthermore, as the available temperature  
 16 data from sensors decreases, there is a decrease in model accuracy for non-flashover instances  
 17 such as  $I_{FO-60}$ , ...,  $I_{FO-40}$ . This parameter study shows that the missing temperature data which  
 18 occurs in real fire scenarios will notably affect the model performance.

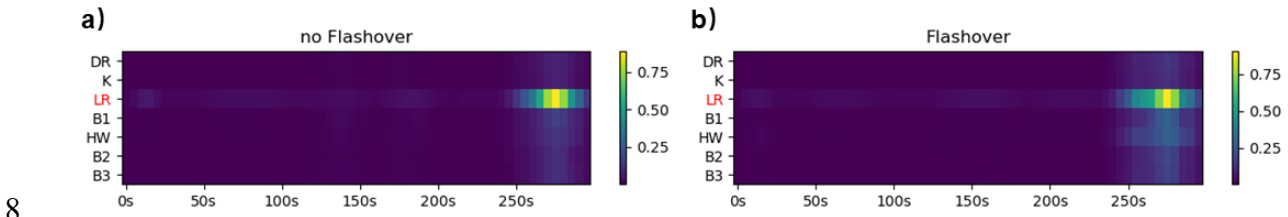


19  
 20 Fig. 8. Detailed model performance of xFlashNet for various HD temperature-limit cases.

21 **4.3 Understanding Discriminative Data to Model Decisions Using dCAM**

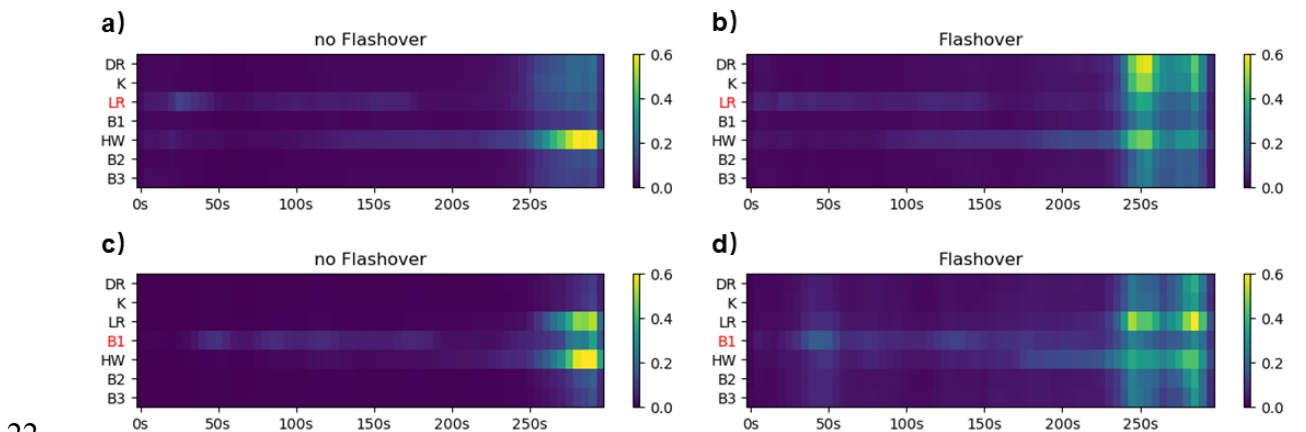
22 Fig. 9 shows the dimension-wise class activation map (dCAM) for non-flashover and flashover  
 23 instances for 30 cases with a fire started in living room (LR). Each dCAM is obtained using  
 24 180 samples (30 fire cases x 6 instances, either non-flashover or flashover, from the same case).  
 25 As shown in the figure, the dimension of dCAM is 60 x 7 in temporal and spatial domain,

1 respectively. Each dCAM element has a weight ranging from 0 to 1. The higher the weight of  
 2 the element is, the more important/discriminative the corresponding temperature information  
 3 is for the model to make the decision. It can be seen in both Fig. 9a and Fig. 9b, the model  
 4 tends to rely on LR HD temperature information in between 250 s to 300 s to decide whether  
 5 there is a flashover and this model behavior is reasonable and expected. To determine flashover,  
 6 although the model does rely mostly on the HD temperature from LR, the HD temperature  
 7 from other compartments (most notably hallway, denoted as HW) are also used.



8  
 9 Fig. 9. dCAM for a) non-flashover and b) flashover instances (no HD temperature limits).

10 Fig. 10 shows the dCAM for LR fire cases (Fig. 9a and b) and bedroom 1 (B1) fire cases (Fig.  
 11 10c and d) with HD maximum operating temperature limit at 300 °C. Similar to Fig. 9, non-  
 12 flashover and flashover instances are used to construct the dCAM and 180 samples are used. It  
 13 is interesting to note that, for LR fire cases, the model uses relatively different temperature  
 14 information to make the decision when HD maximum operating temperature limit is considered.  
 15 For non-flashover cases and as compared to Fig. 9a, Fig. 10a illustrates that the model relies  
 16 more often the HD temperature from HW. This makes sense because the temperature in LR  
 17 exceeds 300 °C and so useful temperature from LR is no longer available. For that, the model  
 18 needs to learn the temperature patterns from other compartments to make correct predictions.  
 19 This model behavior is consistent for non-flashover instances from B1 fire cases as shown in  
 20 Fig. 10c. The figure shows that the model also utilizes temperature from HW and LR to make  
 21 the prediction.



22  
 23 Fig. 10. dCAM for a) LR non-flashover, b) LR flashover, c) B1 non-flashover, and d) B1  
 24 flashover instances with HD maximum operating temperature limit at 300 °C.

25 In terms of flashover instances, since the HD from the room of fire origin generally does not

1 provide any useful temperature readings, it is observed from Fig. 10b and Fig. 10d that the  
2 model also tends to make use of temperature information from adjacent compartments. For the  
3 LR fire cases, the model tends to focus on temperature information from 240 s to 295 s in DR,  
4 K, and HW to make a decision. For the B1 fire cases, the model tends to rely on temperature  
5 from LR. Physically, this is because the HD from HW also exceeds 300 °C soon after in the  
6 B1 fire cases. For that, LR temperature information is used. As seen from Fig. 9b, 10b, and  
7 10d, the temperature from B2 and B3 has relatively less influence for model decision making.  
8 It should be noted that this is because the doors of B2 and B3 are closed in some of the 30  
9 flashover fire cases. Since, the HD temperature is generally at room temperature, the model  
10 neglects this information. Nevertheless, the dCAM is helpful to interpret the model decision  
11 and this is an important step forward to build a more trustworthy ML-based prediction model.

#### 12 4.4 Model Testing on Real Fire Data

13 Given the fact that xFlashNet is developed based on synthetic temperature data, it is necessary  
14 to examine its performance against real fire scenarios. In this study, 11 sets of full-scale  
15 experiments reported in [20] are utilized. The full-scale experiments include 5 living room  
16 (LR), 2 kitchen (K), and 4 bedroom 1 (BR1) fire tests. The building structure is identical to that  
17 shown in Fig. 2.

18 The temperature sequences collected from the 7 sensors near ceiling (3 cm away from ceiling)  
19 in each experiment are pre-processed according to that described in Section 2.2. There are 6  
20 instances for flashover ( $I_{FO-30} \dots I_{FO-5}$ ) and 6 instances for non-flashover ( $I_{FO-60} \dots I_{FO-35}$ ).  
21 In addition, the maximum operational temperature of the sensors is also applied for this  
22 analysis. If the temperature surrounding the sensors exceeds 300 °C, no temperature data will  
23 be seen by the sensors.

24 Table 6 presents the model performance for real fire data. It should be noted that xFlashNet  
25 has not seen these experimental data during the training processing. As shown in Table 6, the  
26 overall performance of the model is quite promising and the average accuracy from all tests is  
27 about 82.5 % with an average accuracy of ~ 88.3 %, ~ 87.4 %, and ~ 72.9 % for LR, K, and  
28 BR1 fire tests, respectively. Table 6 also shows the average accuracy of the individual flashover  
29 instances ( $I_{FO-30} \dots I_{FO-5}$ ) for each test series. It can be seen that the model has relatively high  
30 accuracy for  $I_{FO-20} \dots I_{FO-5}$  instances for the LR and the K fire cases. However, the prediction  
31 accuracy drops on the accuracy for  $I_{FO-30}$  and  $I_{FO-25}$  instances. Also, for BR1 fire cases, the  
32 prediction accuracy for  $I_{FO-30} \dots I_{FO-15}$  instances is generally poor. Comparing the  
33 temperature increase behaviors from fire cases obtained from CFAST and the real fire  
34 experiments, it is found that the sensor temperature obtained from CFAST is generally higher  
35 to that from the real fire experiments. From that, it is believe that the fire data obtained from  
36 CFAST could overpredict the sensor temperature. Therefore, additional studies are needed to  
37 close this knowledge gap and to improve the model robustness on real fire scenarios

38

39 .

Table 6. Prediction accuracy of xFlashNet on real fire data.

Fire Location	Avg.	Non-Flashover	$I_{FO-30}$	$I_{FO-25}$	$I_{FO-20}$	$I_{FO-15}$	$I_{FO-10}$	$I_{FO-5}$
LR (5)	88.3 %	96.6 %	20 %	60 %	100 %	100 %	100 %	100 %
K (2)	87.4 %	91.6 %	50 %	50 %	100 %	100 %	100 %	100 %
BR1 (4)	72.9 %	100 %	0 %	0 %	25 %	25 %	100 %	100 %

## 5. Conclusions

In this present work, an explainable deep learning based flashover prediction model, xFlashNet, is developed for a multi-compartment structure. The model is trained using synthetic temperature data from 17 365 flashover fire cases with a wide range of fire and vent opening conditions. In order to assess the model performance, xFlashNet is benchmarked against three current-state-of-the-art modes. Results show that the proposed model outperforms the benchmark models and it has an overall accuracy of  $\sim 92.9\%$  for predicting if there is a flashover in the next 30 s. The effect of missing data to the model performance is also assessed. Parametric studies demonstrate that the overall model accuracy decreases with decreasing available temperature information. Given the heat detector (HD) maximum operating temperature limit of  $150\text{ }^{\circ}\text{C}$ , the prediction accuracy is reduced to  $\sim 81.9\%$ . Model testing against real fire data is also carried out to examine the model performance and understand the potential knowledge gap for model implementation in real fire scenarios. xFlashNet is tested against data from 11 full-scale fire experiments. The overall model accuracy is about  $82.5\%$ . Results show that additional studies are needed to improve xFlashNet's accuracy and to reduce false negatives. Dimension-wise class activation maps (dCAM) are obtained to understand the data importance to the model decision in both spatial and temporal domains. Three example cases are shown. Based on the dCAM, it is illustrated that, with ideal HDs that never fail, the model tends to use the last 50 s of the temperature information from the room of fire origin to determine whether there is a flashover in 30 s. For HD with a maximum operating temperature limit of  $300\text{ }^{\circ}\text{C}$ , the model tends to use temperature information from adjacent compartments. These observations are encouraging to take a step forward to develop explainable ML based models. It is hoped that this present work can also help to develop trustworthy ML based technology to achieve smart firefighting so that it can help reduce firefighter injuries and deaths.

## References

- [1] Kerber, S. 2012. Analysis of changing residential fire dynamics and its implications on firefighter operational timeframes. *Fire technology*, 48(4), 865-891.
- [2] Peacock, R. D., Reneke, P. A., Bukowski, R. W., & Babrauskas, V. 1999. Defining flashover for fire hazard calculations. *Fire Safety Journal*, 32(4), 331-345.
- [3] Babrauskas, V. 1980. Estimating room flashover potential. *Fire Technology*, 16(2), pp.94-103.

- 1 [4] Stowell, F. M. and Murnane, L. 2017. Essentials of Fire Fighting and Fire Department  
2 Operation. 7th Edition. International Fire Service Training Association.
- 3 [5] McCaffrey, B.J., Quintiere, J.G., Harkleroad, M.F., 1981. Estimating room temperatures  
4 and the likelihood of flashover using fire test data correlations. *Fire Technol.* 17(2), 98–119.
- 5 [6] Kim, H. J., & Lilley, D. 1999. Comparison of theories for room flashover. In 37th  
6 Aerospace Sciences Meeting and Exhibit (p. 343).
- 7 [7] Jahn, W., 2017. Using suppression and detection devices to steer CFD fire forecast  
8 simulations. *Fire Saf. J.* 91, 284–290.
- 9 [8] Nasiri, S., Khosravani, M.R., Weinberg, K., 2017. Fracture mechanics and mechanical  
10 fault detection by artificial intelligence methods: A review. *Eng. Fail. Anal.* 81, 270–293.
- 11 [9] Xiao, Z., Xu, X., Xing, H., Song, F., Wang, X., Zhao, B., 2021a. A federated learning  
12 system with enhanced feature extraction for human activity recognition. *Knowl.-Based Syst.*  
13 229, 107338.
- 14 [10] Ye, X. W., Jin, T., & Yun, C. B., 2019. A review on deep learning-based structural health  
15 monitoring of civil infrastructures. *Smart Struct Syst*, 24(5), 567-585.
- 16 [11] Tang, W., Tam, W.C., Yuan, L., Dubaniewicz, T., Thomas, R. and Soles, J., 2020.  
17 Estimation of the critical external heat leading to the failure of lithium-ion batteries. *Applied*  
18 *thermal engineering*, 179, p.115665.
- 19 [12] Tam, W.C., Yuen, W.W. and Chow, W.K., 2016. Numerical study on the importance of  
20 radiative heat transfer in building energy simulation. *Numerical Heat Transfer, Part A:*  
21 *Applications*, 69(7), pp.694-709.
- 22 [13] Wang, J., Tam, W.C., Jia, Y., Peacock, R., Reneke, P., Fu, E.Y., Cleary, T., 2021. P-flash–  
23 A machine learning-based model for flashover prediction using recovered temperature data.  
24 *Fire Saf. J.* 122, 103341.
- 25 [14] Wu, X., Park, Y., Li, A., Huang, X., Xiao, F., Usmani, A., 2021. Smart detection of fire  
26 source in tunnel based on the numerical database and artificial intelligence. *Fire Technol.* 57  
27 (2), 657–682.
- 28 [15] Kou, L., Wang, X., Guo, X., Zhu, J., & Zhang, H., 2021. Deep learning based inverse  
29 model for building fire source location and intensity estimation. *Fire Safety Journal*, 121,  
30 103310.
- 31 [16] Fu, E.Y., Tam, W.C., Wang, J., Peacock, R., Reneke, P., Ngai, G., Leong, H.V., Cleary, T.,  
32 2021. Predicting flashover occurrence using surrogate temperature data. In: *Proceedings of the*  
33 *AAAI Conference on Artificial Intelligence*, Vol. 35, no. 17. pp. 14785–14794.
- 34 [17] Zhang, T., Wang, Z., Wong, H.Y., Tam, W.C., Huang, X., Xiao, F., 2022. Real-time  
35 forecast of compartment fire and flashover based on deep learning. *Fire Saf. J.* 130, 103579.
- 36 [18] Boniol, P., Meftah, M., Remy, E., & Palpanas, T. 2022. dcam: Dimension-wise class  
37 activation map for explaining multivariate data series classification. In *Proceedings of the 2022*  
38 *International Conference on Management of Data* (pp. 1175-1189).
- 39 [19] Wang, Z., Yan, W., & Oates, T., 2017. Time series classification from scratch with deep  
40 neural networks: A strong baseline. In *2017 International joint conference on neural networks*  
41 *(IJCNN)* (pp. 1578-1585). IEEE.

- 1 [20] Madrzykowski, D. and Weinschenk, C. 2019. Impact of fixed ventilation on fire damage  
2 patterns in full-scale structures. Underwriters Laboratories Firefighter Safety Research Institute.  
3 Columbia, MD.
- 4 [21] Tam, W. C., Fu, E. Y., Peacock, R., Reneke, P., Wang, J., Li, J., & Cleary, T., 2020.  
5 Generating synthetic sensor data to facilitate machine learning paradigm for prediction of  
6 building fire hazard. *Fire technology*, 1-22.
- 7 [22] Reneke, P. A., Peacock, R. D., Gilbert, S. W., & Cleary, T., 2021. CFAST—Consolidated  
8 Fire and Smoke Transport (Version 7) Volume 5: CFAST Fire Data Generator (CData). NIST  
9 TN 1889v5. National Institute of Standards and Technology, Gaithersburg, MD.
- 10 [23] Peacock, R. D., Forney, G. P., & Reneke, P. A., 2015. CFAST—consolidated fire and  
11 smoke transport (version 7)—volume 3: verification and validation guide. NIST Technical  
12 Note 1889v3. National Institute of Standards and Technology, Gaithersburg, MD.
- 13 [24] Babrauskas, V. and Peacock, R.D. 1992. Heat release rate: the single most important  
14 variable in fire hazard. *Fire Safety Journal* 18(3): 255-272.
- 15 [25] Babrauskas, V., Peacock, R.D. and Reneke, P.A., 2003. Defining flashover for fire hazard  
16 calculations: Part II. *Fire Safety Journal*, 38(7), pp.613-622
- 17 [26] Babrauskas, V., 2011. Glass breakage in fires. Fire Science and Technology, Inc.:  
18 Issaquah, WA.
- 19 [27] Hurley, M.J., Gottuk, D.T., Hall Jr, J.R., Harada, K., Kuligowski, E.D., Puchovsky,  
20 M., Watts, J.M., Wieczorek, C.J. (Eds.), 2015. SFPE Handbook of Fire Protection Engineering.  
21 Quincy, Massachusetts.
- 22 [28] NFPA 72 National Fire Alarm Code 2002 Edition
- 23 [29] He, K., Zhang, X., Ren, S., & Sun, J., 2016. Deep residual learning for image recognition.  
24 In Proceedings of the IEEE conference on computer vision and pattern recognition (pp. 770-  
25 778).
- 26 [30] Yuen, R. K., Lee, E. W., Lo, S. M., & Yeoh, G. H., 2006. Prediction of temperature and  
27 velocity profiles in a single compartment fire by an improved neural network analysis. *Fire  
28 safety journal*, 41(6), 478-485.

29

30 **Figure captions**

31 Fig. 1. a) Screenshot of the full-scale experiment from the residential home [17] and b) CFAST  
32 simulation run for the residential home.

33 Fig. 2. Overview of a) the single story structure and b) openings with heat detectors (HD).

34 Fig. 3. a) Four-stage fire growth curve and b) an example of a fire case.

35 Fig. 4. a) Temperature profiles for a flashover fire case and b) an illustration of a sliding  
36 window with a window size of  $w$ .

37 Fig. 5. a) Zoom-in plot of Fig. 4a and b) temperature profiles of the same case with HD  
38 maximum operational temperature at 300 °C.

- 1 Fig. 6. a) Overall model structure of xFlashNet, b) structure of a residual block, and c)
- 2 information flow to obtain the dimension-wise class activation map.
- 3 Fig. 7. dCAM determination process.
- 4 Fig. 8. Detailed model performance of xFlashNet for various HD temperature-limit cases.
- 5 Fig. 9. dCAM for a) non-flashover and b) flashover instances with no HD temperature limits.
- 6 Fig. 10. dCAM for a) LR non-flashover, b) LR flashover, c) B1 non-flashover, and d) B1
- 7 flashover instances with HD maximum operating temperature limit at 300 °C.